Neuron
Article

Activity-Dependent Clustering of Functional Synaptic Inputs on Developing Hippocampal Dendrites

Thomas Kleindienst,[1,2,3] Johan Winnubst,[1,3] Claudia Roth-Alpermann,[2,4] Tobias Bonhoeffer,[2] and Christian Lohmann[1,2,*]
[1]Netherlands Institute for Neuroscience, 1105 BA Amsterdam, The Netherlands
[2]Max-Planck Institute of Neurobiology, 82152 Martinsried, Germany
[3]These authors contributed equally to this work
[4]Present address: Bernstein Center for Computational Neuroscience, Humboldt University, 10115 Berlin, Germany
*Correspondence: c.lohmann@nin.knaw.nl
DOI 10.1016/j.neuron.2011.10.015

SUMMARY

During brain development, before sensory systems become functional, neuronal networks spontaneously generate repetitive bursts of neuronal activity, which are typically synchronized across many neurons. Such activity patterns have been described on the level of networks and cells, but the fine-structure of inputs received by an individual neuron during spontaneous network activity has not been studied. Here, we used calcium imaging to record activity at many synapses of hippocampal pyramidal neurons simultaneously to establish the activity patterns in the majority of synapses of an entire cell. Analysis of the spatiotemporal patterns of synaptic activity revealed a fine-scale connectivity rule: neighboring synapses (<16 μm intersynapse distance) are more likely to be coactive than synapses that are farther away from each other. Blocking spiking activity or NMDA receptor activation revealed that the clustering of synaptic inputs required neuronal activity, demonstrating a role of developmentally expressed spontaneous activity for connecting neurons with subcellular precision.

INTRODUCTION

During brain development neurons establish highly specific synaptic connections with each other. This process is not only regulated by molecular factors that determine, for example, the formation of connections in specific laminae of brain structures, but also by synaptic activity itself (Cline, 2003; Goodman and Shatz, 1993; Sanes and Yamagata, 2009). In particular, the fine tuning of synaptic connectivity relies on activity-dependent mechanisms that require spontaneous activity that is generated in developing neuronal networks before an organism receives sensory inputs, as well as—later on—activity, which is evoked by sensory experience (Hua and Smith, 2004; Huberman et al., 2008; Katz and Shatz, 1996).

Spontaneous activity has been measured in many brain areas during development and it occurs in the form of repetitive activation of large populations of neurons (Ben-Ari et al., 1989; Galli and Maffei, 1988; Garaschuk et al., 1998; O'Donovan et al., 1994; Wong et al., 1995; Yuste et al., 1992). Frequently, this form of activity travels across brain regions as waves activating neighboring neurons simultaneously. This particular property of intrinsically generated activity in developing networks is thought to be an important component of the activity-dependent establishment of specific brain circuits. For example, the high degree of correlation between neighboring neurons helps maintaining their spatial relationship through ascending neuronal pathways and thus establishing a topographic organization at all levels (e.g., Triplett et al., 2009).

Although the patterns of spontaneous activity at the level of networks and individual neurons have been described in great detail, the activity patterns at the level of individual synapses within the dendritic arborization of single neurons are not known. It has been clear for some time that—within one neuron—spontaneous network events are frequently manifested as barrages or bursts of coincident synaptic inputs (Ben-Ari et al., 1989). However, how these synaptic inputs are distributed across the dendritic tree has not been investigated, mostly due to the fact that electrophysiological measurements do not allow identifying the dendritic locations of synaptic inputs.

In mature neurons, the location of synaptic inputs within the dendritic arborization is most likely crucial for processing and storing information. For example, in tadpoles the dendrites of individual tectal neurons receive topographically organized afferent inputs (Bollmann and Engert, 2009). In mice, pyramidal neurons of the visual and auditory cortex receive functionally diverse synaptic inputs that are integrated by the postsynaptic cell to generate highly specific output (Chen et al., 2011; Jia et al., 2010). Dendritic integration in pyramidal neurons has been shown to be supra-linear and—as a consequence—the simultaneous activation of several synapses that are located close to each other on the same dendrite have a stronger influence on neuronal firing than the activation of the same number of synapses on different branches (Branco and Häusser, 2010; Larkum and Nevian, 2008; Losonczy and Magee, 2006; Polsky et al., 2004). Furthermore, theoretical work demonstrated that such a local integration scheme where information is computed

in dedicated dendritic subunits can boost the information processing capacities of neurons dramatically (Häusser and Mel, 2003; Poirazi and Mel, 2001; Spruston, 2008). Here, we asked whether the patterns of synaptic input that developing hippocampal pyramidal neurons receive during spontaneous network bursts may already reflect such a subcellular fine-scale organization.

By imaging transmission events in large populations of identified synapses, we observed that during each spontaneous burst a different set of synapses is activated. Careful analysis revealed a clear principle underlying the fine-scale organization of these inputs: synapses that are located near each other on the same dendritic branch exhibit a higher degree of temporal correlation than synaptic pairs on different dendrites. By blocking action potential firing or N-methyl-D-aspartate (NMDA) receptor activation in slices for several days we showed that this clustering of synaptic inputs is activity-dependent. Thus, by quantifying and comparing a large population of functional synaptic inputs across the dendritic arborization (the "synaptome"; DeFelipe, 2010) of developing pyramidal neurons, we revealed that developing synapses are functionally clustered on developing dendrites and that clustering requires spontaneous activity.

RESULTS

To monitor the spatiotemporal patterns of spontaneous synaptic activation in developing neurons we performed simultaneous patch-clamp recordings and calcium imaging of hippocampal CA3 pyramidal neurons in organotypic slices from neonatal rats (postnatal [P] 0–2, days in vitro [DIV] 2–4). Patch-clamp recordings in voltage-clamp mode revealed spontaneously occurring synaptic currents, most likely representing unitary synaptic events (1.8 ± 0.62 Hz; mean ± standard deviation [SD] per cell), as well as bursts of synaptic inputs, previously described as giant depolarizing potentials (GDPs; Ben-Ari et al., 1989; Bonifazi et al., 2009). We determined the occurrence of bursts using an adapted version of the Rank Surprise method (Gourévitch and Eggermont, 2007; for details see Experimental Procedures). Bursts of synaptic inputs occurred at a rate of 15.02 ± 2.06 min^{-1}, which is in the range measured in previous in vitro and in vivo recordings (Ben-Ari et al., 1989; Leinekugel et al., 2002). In fact, the distribution of burst interevent intervals (Figure S1 available online) was virtually identical to that previously described in the hippocampus of developing rats in vivo (P4–6; Leinekugel et al., 2002), demonstrating that not only the general connectivity (Frotscher et al., 1990; Stoppini et al., 1991), but also fundamental functional parameters are maintained in the hippocampal slice culture preparation.

Calcium imaging in apical dendrites within *stratum radiatum* and *stratum pyramidale* (<200 μm from the soma) revealed spontaneous local calcium transients that occurred at an average rate of 68 ± 43.8 min^{-1} mm^{-1} dendrite (Figure 1A). The majority of local calcium transients were observed in dendritic shafts and not in spines, because there are only very few spines present on dendrites of CA3 pyramidal neurons during this developmental period. Global calcium transients, which can also occur spontaneously in developing CA3 pyramidal neurons and depend on action potential firing, were not observed, since the membrane potential was clamped at −55 mV, the resting membrane potential of neonatal CA3 pyramidal neurons (Safiulina et al., 2006; Sipilä et al., 2006).

Calcium Transients Report Glutamatergic Synaptic Transmission Events

We investigated the possibility that calcium transients that occurred simultaneously with synaptic currents (Figure 1A) represent synaptic transmission at the respective dendritic locations. Electrical stimulation of presynaptic axons triggered both synaptic currents as well as local calcium transients (Figure 1B) whose spatial extent and duration (17.6 ± 13.8 μm and 1.6 ± 1.0 s, respectively; n = 29 transients in three cells) were indistinguishable from those of the spontaneous transients that coincided with synaptic currents (extent: 20.9 ± 19.8 μm; duration: 1.3 ± 1.0 s, n = 3,160 transients in eight cells). The durations of synaptic calcium transients were in the upper range of previously reported values (Murphy et al., 1994; Murthy et al., 2000), probably because NMDA mediated synaptic currents in young hippocampal pyramidal neurons exhibit longer decay times than in mature cells (Hsia et al., 1998). While approximately one half (56 ± 31%) of all local calcium transients coincided with synaptic currents, we also observed calcium transients that occurred in the absence of synaptic currents (Figure 1C).

To confirm that the observed coincidence between a subpopulation of spontaneous local calcium transients and the synaptic currents was not accidental, we plotted a histogram of the time differences between the onsets of all local calcium transient and synaptic currents of each recording (61 recordings, 11 cells; Figure 1D). This histogram shows a clear peak at zero demonstrating a systematic relationship of both phenomena. In a control plot, in which we reversed the time axis of calcium transient onsets for each recording, the peak at zero was absent (Figure 1D, inset), indicating that this relationship was not due to periodicities in the occurrence of calcium transients and synaptic currents. Furthermore, blocking NMDA and non-NMDA ionotropic glutamate receptors with APV and NBQX abolished the coincidence between calcium transients and the remaining, most likely GABAergic, synaptic currents (Figure 1E). The delta time curve (Figure 1D) was symmetrical and did not show a fast onset combined with a slow decay as one may have expected. The symmetrical shape of the delta time curve was an effect of the duration of synaptic bursts, during which most calcium transients coinciding with synaptic currents occurred (82 ± 15%). Bursts were the sum of many individual synaptic currents distributed over several hundred milliseconds (367 ± 206 ms). Thus, each calcium transient did not only coincide with one particular synaptic current during a burst, but was also likely to be preceded and followed by synaptic currents that occurred during the same burst.

Next, we mapped synaptic calcium transients along entire dendrites (Figure 1F). For each site where calcium transients occurred we determined the percentage of transients that coincided with synaptic currents. For comparison we also estimated the likelihood of coincidence that would occur by chance for each neuron, given its frequencies of calcium transients and synaptic currents. We defined a dendritic site as synaptic based on the ratio of actual over by-chance coincidence. We plotted

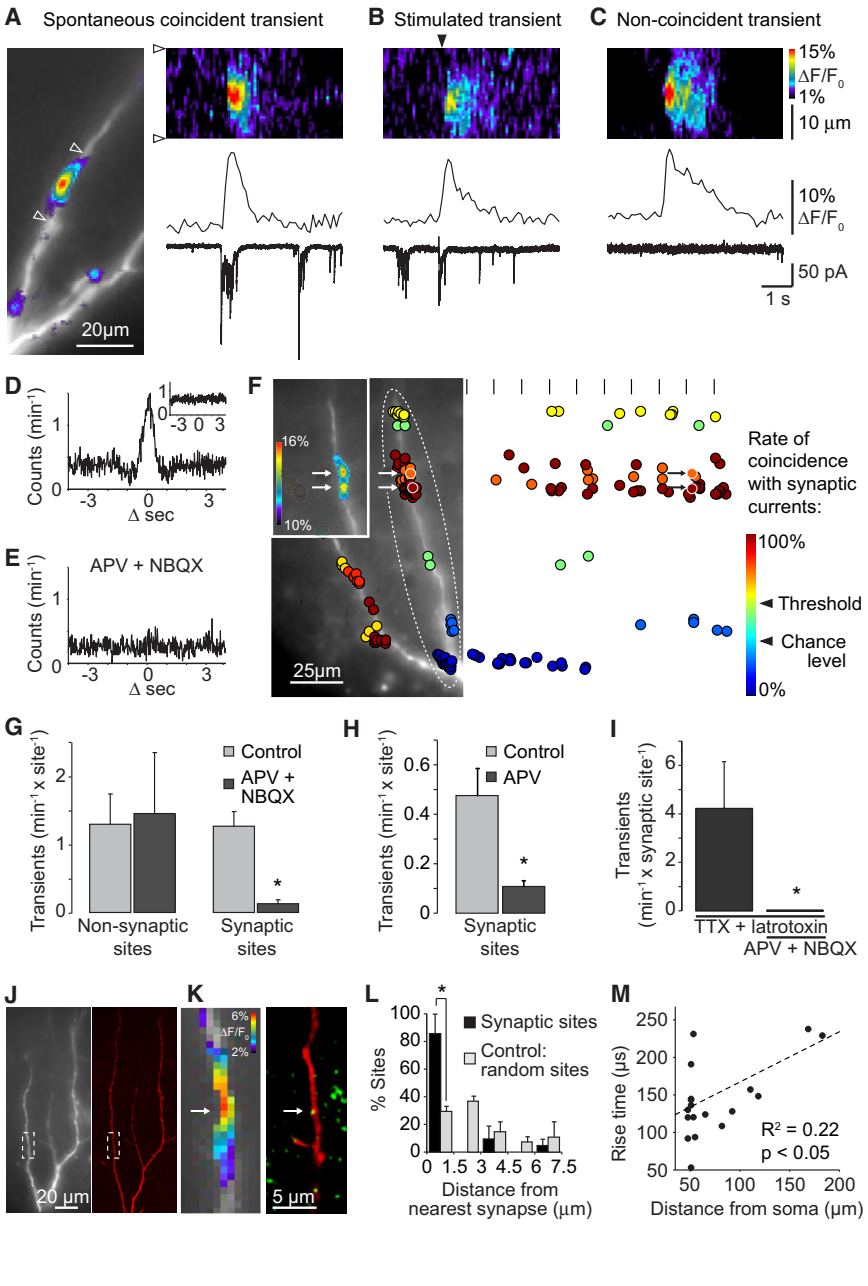

Figure 1. Dendritic Calcium Transients at Synaptic and Nonsynaptic Sites

(A) Apical dendrite of a CA3 pyramidal neuron. A spontaneous local calcium transient is superimposed onto the dendrite. $\Delta F/F_0$ values are represented in pseudo color. Arrowheads indicate the extent of the measured dendritic segment used for the pseudo line-scan of this transient (right). Traces show changes in $[Ca^{2+}]_i$ as $\Delta F/F_0$ and simultaneous voltage-clamp recording.

(B) Dendritic calcium transient after presynaptic stimulation in a different cell (arrow head: presynaptic stimulation).

(C) Calcium transient that does not coincide with a synaptic current event.

(D) Histogram of time differences between the onsets of calcium transients and electrophysiological events demonstrates a high prevalence of co-occurrence. Inset shows histogram calculated with reversed time axis of calcium transients as a control.

(E) The histogram of time differences in the presence of the glutamate receptor antagonists APV and NBQX does not show a detectable peak.

(F) Spatiotemporal mapping of dendritic calcium transients. Each dot marks the center of one calcium transient. Each transient is represented twice to show its location (left) as well as its time point of occurrence (right). For two calcium transients that occurred simultaneously (arrows, light gray outline) the respective calcium rises are shown in pseudo color (inset). All calcium transients that putatively occurred at identical locations were assigned to a particular site (for details see Experimental Procedures). All transients that occurred at a given site were labeled with a color that denotes the fraction of calcium transients at this particular site that coincided with synaptic currents. In the time representation (right) each vertical line marks the onset of a 2 min recording. The chance level of coincidence and the threshold for synaptic sites (1.5 times the chance level) are indicated at the scale bar.

(G) Calcium activity at synaptic sites—but not at nonsynaptic sites—was significantly reduced in the presence of APV + NBQX.

(H) Calcium activity at synaptic sites was significantly reduced in the presence of APV.

(I) In the absence of network activity, unitary synaptic calcium transients triggered by latrotoxin stimulated synaptic release were entirely blocked by APV + NBQX.

(J–L) Post-hoc immunohistochemistry with synapsin antibodies demonstrated that functional synapses were located at dendritic sites, which were opposed to synapsin positive puncta. (J) Pyramidal neuron during the live experiment and after fixation (red). (K) A synaptic calcium transient occurred at a site opposed to a synapsin labeled presynaptic terminal (arrows). The confocal image (right) represents a single plane where the synapsin positive structure (green) is directly contacting the dendrite (red). (L) More than 85% of all dendritic sites that were identified as functional synapses were located within 1.5 μm of a synapsin stained presynaptic terminal.

(M) The rise time of synaptic currents correlated with the distance of each synaptic site from the soma. All error bars represent standard error of the mean (SEM).

a histogram of this ratio for all dendritic sites where calcium transients occurred (Figure S2). As expected, many values clustered around the estimated chance level. There was a clear dip around 1.5 times the chance level, most likely separating the nonsynaptic from the synaptic population. We fitted the data around one with a Gaussian (assuming a normal distribution) and found that <5% of nonsynaptic sites would have ratios of >1.5. Therefore, we defined synaptic sites as those where the rate of coincidence was more than 1.5 times higher than the coincidence expected purely by chance and used this value to distinguish between putative synaptic and nonsynaptic sites. This measure effectively separated synaptic from nonsynaptic calcium transients, since the activity at sites defined as putatively synaptic was almost entirely silenced by APV (50 μM)

and NBQX (10 μM), whereas the activity at sites identified as nonsynaptic was not affected by the glutamate receptor antagonists (Figure 1G). APV alone abolished 80% of synaptic calcium transients (Figure 1H) without significantly affecting the frequency of bursts (baseline: 33 ± 8/min; APV: 30 ± 7 /min; $p > 0.05$, $n = 5$ cells) or the amplitudes of synaptic currents (baseline: −54 ± 11 pA; APV: −46 ± 9 pA; $p > 0.05$, $n = 5$ cells), demonstrating that calcium flux through NMDA receptors was the major contributor to these synaptic calcium transients.

To demonstrate directly that individual synaptic calcium transients reported glutamatergic transmission events, we recorded calcium transients after blocking network activity with TTX and enhancing synaptic release with latrotoxin. After additional wash-in of APV and NBQX synaptic calcium activity was completely abolished in six out of six experiments, indicating that synaptic calcium transients were entirely dependent on glutamate receptor activation (Figure 1I). Nonsynaptic calcium transients persisted. Our previous studies indicated that nonsynaptic calcium transients can be triggered by very diverse factors, such as BDNF signaling and the formation of new contacts between dendrites and axons, possibly through adhesion molecules (Lang et al., 2007; Lohmann and Bonhoeffer, 2008). The following analyses were focused on synaptic calcium transients.

Since synaptic bursts in the hippocampus require also GABAergic signaling (Ben-Ari et al., 1989; Khalilov et al., 1999), we blocked GABA receptors using picrotoxin (150 μM) within the otherwise active network. We observed, as expected, a significant reduction of the burst frequency (baseline: 6.7 ± 1.5 /min, picrotoxin: 1.8 ± 0.5 /min, $p < 0.05$). The remaining bursts were characterized by very high amplitudes and numbers of active synapses. They were reminiscent of interictal epileptiform bursts that have been observed previously in the absence of GABA signaling in developing CA3 pyramidal neurons (Khalilov et al., 1999). Since the number of active synapses was particularly high during these interictal events, the overall frequency of synaptic calcium transients did not change significantly (baseline: 0.31 ± 0.10 /min; picrotoxin: 0.48 ± 0.10 /min, $p > 0.05$). Although these results demonstrate that GABA receptor activation is required for regular bursting, they are in line with our previous conclusion that GABA signaling does not contribute to synaptic calcium transients as measured here.

The results above showed that local calcium transients, which coincided with synaptic currents, could be used as reliable reporters of glutamatergic synaptic transmission events. Post-hoc immunohistochemistry supported this conclusion. More than 85% of sites that had been identified as functional synapses were located at synapsin labeled presynaptic structures ($n = 3$ cells; Figures 1J–1L). This analysis revealed in addition that functional synapses were identified at approximately one quarter (23.5 ± 4.9%, SD) of synapsin labeled sites. Considering that some of the labeled puncta may have been in contact with the imaged dendrite within the resolution of light microscopy, but actually represented synapses on different dendrites, we probably underestimated the fraction of functional versus structural synapses somewhat. Labeling with a GAD65 antibody, a marker of GABAergic synapses, demonstrated that 43% (±3.2%, SD) of synapsin labeled sites represented inhibitory synapses, which is within the range previously reported for developing hippocampal neurons in culture (30%–50%; Benson et al., 1994; Zhao et al., 2005). Thus, we mapped activity of at least 42% of the structurally identified excitatory synapses. The remaining population comprised probably silent synapses and synapses that were not active during the recording period or not active often enough to identify them as synaptic based on their rate of coincidence with synaptic currents. Together, we conclude that our approach identifies a large proportion of a neuron's functional glutamatergic synapses.

While most synaptic calcium transients occurred during bursts, some coincided with unitary synaptic currents (18 ± 15%, SD). In the latter cases we could frequently assign synaptic currents directly to individual synaptic sites. We took advantage of this information to investigate whether the kinetics of synaptic currents depended on the position of individual synapses along the dendrite. Specifically, we measured the rise times of unitary spontaneous synaptic currents and observed that they were longer at distal synapses than at more proximally located synapses (Figure 1M) as described previously for hippocampal pyramidal neurons (e.g., Smith et al., 2003). This observation further strengthened the conclusion that local calcium transients reported synaptic transmission events reliably.

Spatial Distribution of Functional Synaptic Inputs: The Synaptome

Having established a contingent of dendritic calcium transients as indicators of synaptic transmission, we determined the spatiotemporal patterns of synaptic activation across large parts of the dendritic tree, the synaptome. We imaged over large tissue volumes containing the major part of the dendritic arborization of individual neurons. Frame rates of 30 Hz and simultaneous stepping across different focal planes enabled us to acquire stacks of three images over a total depth of 20 μm in 100 ms, resulting in an acquisition rate of 10 Hz over a large part of the dendritic tree of a pyramidal neuron. Recording for several minutes at four different locations of the cells shown in Figure 2 was sufficient to map synaptic activity and the sites of active synapses in 70%–90% of their dendritic arborization. This demonstrated that while synaptic transmission occurred even at the most distal apical dendrites, the frequency and density of synaptic inputs was higher in the primary apical and the proximal basal dendrites.

We quantified the distribution of synaptic activity in the dendritic arborization across seven cells. To make these numbers comparable, we chose an approach analogous to the Sholl diagram that is often used for the analysis and comparison of neuronal complexity (Sholl, 1953). While for the classical Sholl diagram the relevant parameter is the number of intersections between dendrites and concentrically arranged circles around the soma (Figures 3A and 3B), our functional Sholl analysis sums the number of synaptic events per minute for dendritic areas of increasing distance from the soma (Figures 3C and 3D). The general distribution of dendritic branches and synaptic inputs was similar; however, some clear differences between the functional and structural diagrams were apparent. For example: while the density of branches within the most proximal areas of the apical dendritic field is low, synaptic activity is high in

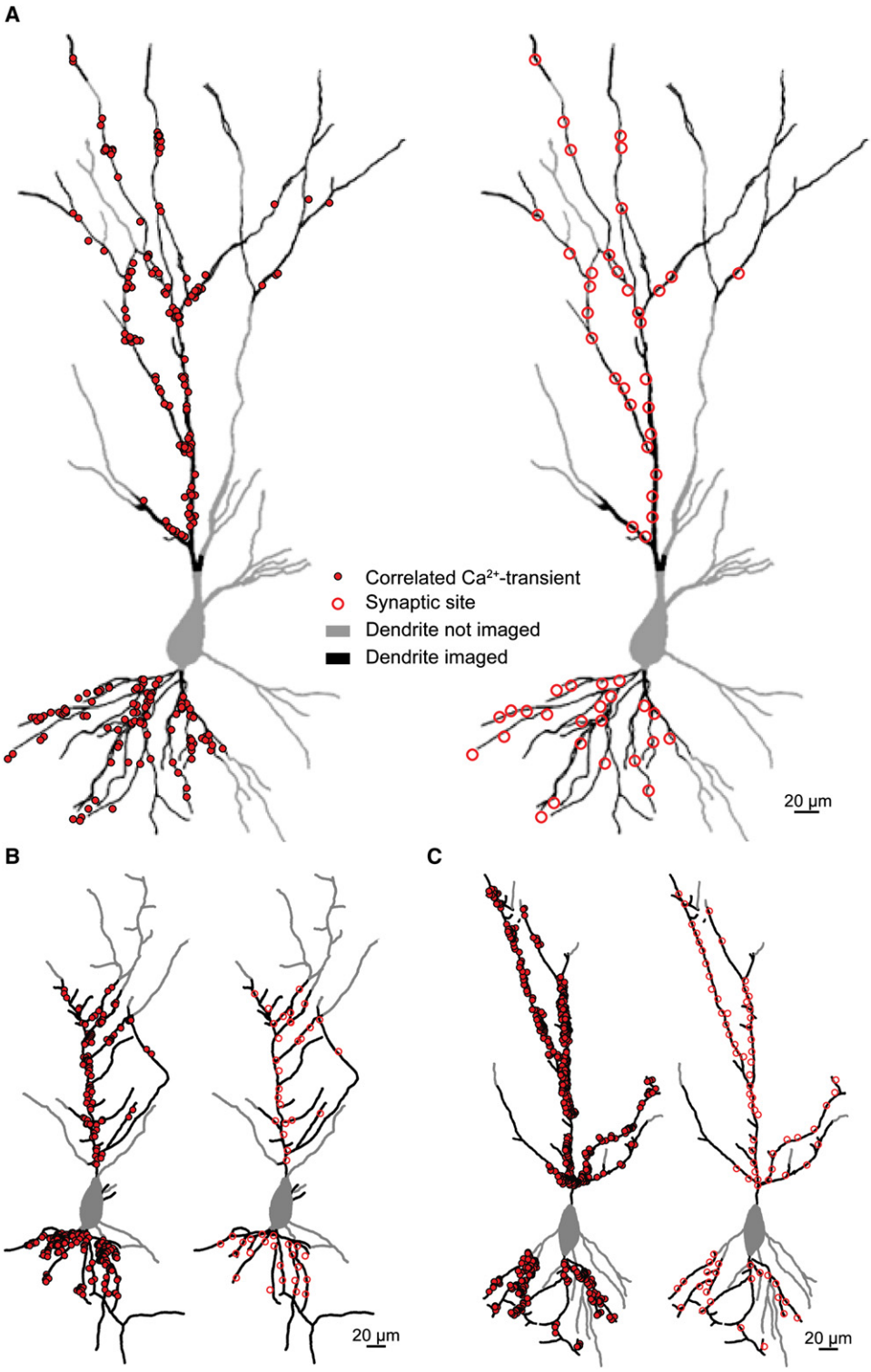

Figure 2. Mapping the Synaptome in Three CA3 Pyramidal Neurons
For each cell calcium transients that coincided with synaptic currents (red dots) are shown on the left and synaptic sites (red circles) on the right.

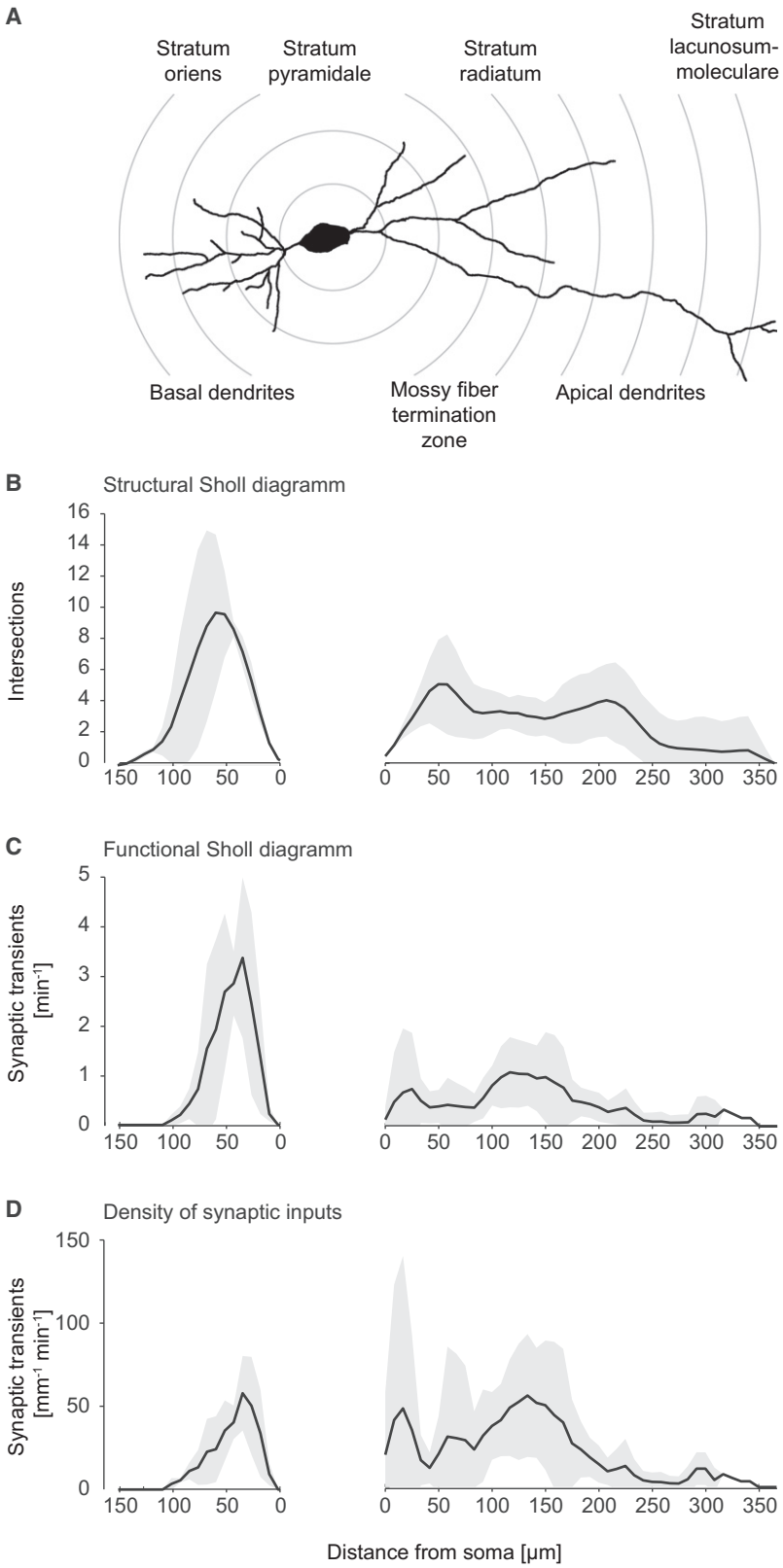

Figure 3. Structural and Functional Sholl Diagrams

(A) Example pyramidal neuron.

(B) Structural Sholl diagram: numbers of intersections between dendrites and imaginary circles at increasing distances from the soma. Black lines show mean of seven and three pyramidal cells for the apical and basal arborizations, respectively; gray areas represent mean ± standard deviation (SD).

(C) Functional Sholl diagram for the same cells as in (B). Synaptic transients per minute for increasing distances from the soma.

(D) Density of synaptic inputs: synaptic transients normalized to the length of dendrite in each distance bin.

absolute as well as relative terms. The highest density of synaptic inputs was measured in the basal dendrites, in the most proximal apical dendrites and in apical dendrites spanning a 50–100 μm wide region distal from the mossy fiber termination zone within *stratum radiatum*. We observed the lowest density of synaptic inputs in the most distal apical dendrites (>200 μm from the soma). One possibility is that we underestimated the number of distal synapses due to an attenuation of their currents in the dendrite. In this case, one would expect to find a strongly reduced proportion of synaptic calcium transients in distal dendrites compared to proximal ones, because one would falsely identify synaptic transients as nonsynaptic. However, the proportion of calcium transients that were identified as synaptic within the total population was similar (or even higher) in distal apical dendrites compared to proximal dendrites (proximal, < 200 μm: 59 ± 9%; distal, > 200 μm: 74 ± 17%, not significant). Furthermore, the activity at distant sites (>160 μm from the cell body) that were classified as nonsynaptic was low and not affected by APV and NBQX (before: 0.16 ± 0.07/min, after 0.18 ± 0.05/min, n = 4, not significant), demonstrating that we did not falsely classify synaptic sites as nonsynaptic at these distal locations. Together, this data shows that we sampled synaptic calcium transients at all locations across the dendritic arborization equally well.

Spatiotemporal Patterns of Synaptic Activation

After determining the spatial distribution of synaptic inputs onto developing pyramidal neurons, we sought to determine the spatiotemporal patterns of synaptic activity across the dendritic arborization. We investigated how synaptic inputs are distributed during successive GDPs. We found that the patterns of activation differed from burst to burst (Figures 4A–4C). As expected, the number of synapses that were activated during each burst correlated significantly with the total charge transfer per burst in this cell (Figures 4B–4D) and in the entire population ($R^2 = 0.1$, $p < 0.05$, n = 7 cells). Next, we asked whether a certain structure could be detected in these activation patterns. We observed frequently that neighboring synapses were coactive (e.g., Figure 1F; synaptic pairs 1/2 and 3/4 in Figures 4A and 4B and Figure 5A). Therefore, we analyzed the relationship between coactivity of two synapses and the distance between these synapses along the dendrite. First we verified that a pair of nearby synapses could be activated together or separately at different times during the recording (Figure 5B). The activity at pairs of synapses with an intersynaptic distance of 10 μm and less could be reliably distinguished and assigned to their respective site (Figure 5B). We then analyzed manually the rate of simultaneous activation (within a period of 100 ms) for all 14 synapses (91 pairs) over a total recording period of 16 min in one neuron. This analysis revealed a high degree of coactivation in neighboring pairs (Figure 5C). In contrast, the likelihood of coactivation was very small in pairs of synapses that were separated by more than 16 μm. To analyze the large amount of data from the entire set of cells (n = 10), we implemented an automated analysis. We chose conservative thresholds for both, the detection of synaptic calcium transients and for separating simultaneous synaptic calcium transients at neighboring sites to keep the rate of false positives low. Even though the absolute

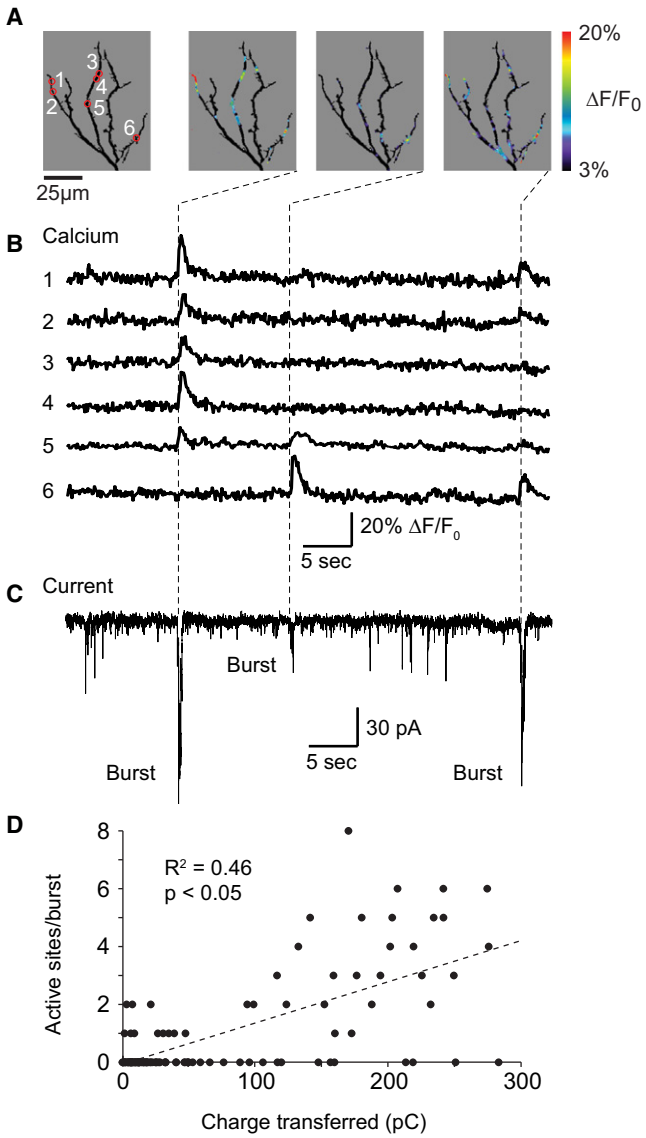

Figure 4. Contribution of Individual Synapses to Bursts of Synaptic Input

(A) Synaptic sites (left) and their activation patterns during successive bursts of synaptic input.

(B) Traces show $\Delta F/F_0$ for six synaptic sites shown in (A).

(C) Voltage clamp recording: three bursts of simultaneous synaptic events are marked. A different set of synapses contributed to each burst.

(D) Relationship between burst size (charge transferred) and the number of active synapses in the neuron shown in (A–C). Dashed line shows linear fit.

values obtained with the automated analysis across all cells were lower—as expected due to the conservative thresholds—qualitatively they showed the same result as the manual analysis of an individual cell: synapses that are located close to each other are more likely to be coactive than more distant synapses (Figure 5D).

The average rate of coactivation was significantly higher at intersynapse distances of 0–8 μm (7.44 ± 2.2% standard error

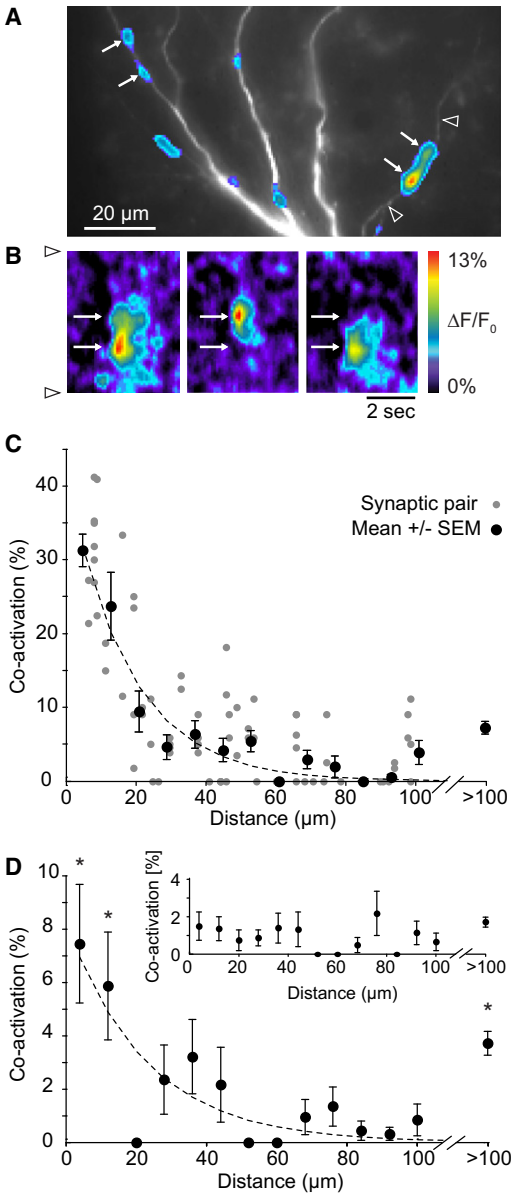

Figure 5. Coactivation of Neighboring Synapses

(A) Synaptic calcium transients during one burst. Note that two pairs of neighboring synapses are coactive (arrows, intersynapse distances: left, 14 µm; right, 10 µm).

(B) Pseudo linescans of calcium transients in the dendritic segment marked with arrowheads in (A). Both synapses were coactive at the first time point and each was active individually at the second and third time point, showing that activity at neighboring sites can be assigned to each synapse (mean filtered).

(C) Relationship between intersynaptic distance and prevalence of co-activation for all synapse pairs of one cell. Manual analysis. Dotted line: nonlinear fit (Nelder-Mead).

(D) Graph as in (B) for the entire experimental set (n = 10 cells). Automated analysis. Asterisks indicate significant differences between individual data points and the mean of all sites. Inset, control: graph as in (B) for a specific delay (200–300 ms) between synaptic transients at each synapse pair instead of simultaneous activation. No relationship with intersynapse distance could be observed, indicating that the time window for correlation between neighbors was <200 ms. All error bars represent SEM.

of the mean [SEM], automated analysis) and 8–16 µm (5.49 ± 1.9% SEM) compared to the entire population (2.65 ± 0.26% SEM, n > 40 synapse pairs for each distance group). Very distant synapse pairs (>100 µm) were also significantly more coactive than the mean population (see also below), but significantly less coactive than very close synaptic pairs (<16 µm). The likelihood of successive activation at a specific delay (for example: 200–300 ms) was not dependent on the intersynapse distances (Figure 5D, inset) demonstrating that the distance-dependence of synaptic activation is indeed specific for coactivation within 200 ms or less.

The high prevalence of correlated activity at neighboring synapses could arise from individual axons making more than one synapse onto a given dendrite within short distances. Our anatomical and functional analyses showed that this is very unlikely for two reasons. First, a new analysis of our previous anatomical data from the same developmental stage (Lohmann and Bonhoeffer, 2008) revealed that axons (>200, n = 7 cells) passed individual dendrites in a near orthogonal angle and 43 axons had one contact with a particular dendrite, but none had more than one. Second, minimal stimulation of presynaptic axons (Figure 1B) never triggered responses at more than one synapse within 16 µm along the dendrite (n = 5 cells, six sites, 120 stimulation events). The latter observation also ruled out another possible explanation for coactivation, namely spill-over of glutamate or diffusion of intra- or extracellular signaling factors as a consequence of activation of one synapse. Finally, we examined whether coactivation of neighboring synapses might be the consequence of a clustered distribution of synapses. We measured the intersynapse distances of both, anti-synapsin labeled synapses and synapses mapped with calcium imaging. We found that synapses are distributed largely independently from each other, and showed rather a neighbor exclusion zone than clustering in both cases (Figure S3).

Together these observations demonstrated that the synaptic inputs of CA3 pyramidal neurons were spatiotemporally structured. Specifically, the likelihood of being coactive within 100 ms was higher for pairs of synapses whose intersynapse distance was within 16 µm.

The Fine-Scale Organization of Functional Synaptic Inputs Is Activity-Dependent

We speculated that the fine-scale organization of synaptic inputs onto developing CA3 pyramidal neurons may be a consequence of an activity-dependent sorting process, where synapses with presynaptic axons that spike simultaneously get specifically stabilized, if they are located near each other along the dendrite. To test whether spiking activity is indeed required for establishing or maintaining the input organization, we performed an additional set of experiments. Hippocampal slices from the same animals were randomly placed in culture wells that contained control medium—as used for the experiments described above—or medium that contained tetrodotoxin (TTX; 1 µM) a sodium channel blocker to prevent action potential firing during incubation. After 3–4 days of incubation in control or TTX medium, slices where transferred to regular recording medium (without TTX) and the distribution of functional inputs was determined alternately in control and TTX treated pyramidal cells.

Neither the frequency of bursts (control: 15.02 ± 2.06 min^{-1}, TTX: 17.92 ± 1.23 min^{-1}), the frequency of local calcium transients per synapse (control: 0.58 ± 0.09 min^{-1}, TTX: 0.72 ± 0.11min^{-1}), nor the density of functional synapses (control: 39.5 ± 14.8 mm^{-1}, TTX: 57.6 ± 23.6 mm^{-1}) was significantly different between control and TTX treated cells. And, as expected, the fine-scale organization of synaptic inputs in control cells was indistinguishable from that in our first set of experiments (compare Figure 5C and Figure 6).

In contrast, the relationship between distance and input correlation was entirely abolished in cells that developed in the absence of neuronal spiking (Figure 6A). Interestingly, we observed not only a significant reduction of coactivation at neighboring synapses, but also an increase in coactivation in synapse pairs of intermediate distances (50–100 μm). This suggested that spiking activity led to the stabilization of neighboring coactive synapses and a depletion of synapses that are coactive at intermediate distances. The latter conclusion is further supported by the observations that very distant synapse pairs (>100 μm) exhibit higher correlations than those of intermediate distance (Figures 5D and 6A) and that the correlation of very distant synaptic pairs was identical in TTX treated and control cells (Figure 6A). Finally we investigated whether NMDA receptors, which mediate calcium signaling at the synapse (Figure 1H), but are dispensable for bursting, are required for the activity-dependent development of synaptic clustering. Slices were incubated in medium containing APV for 3–4 days. Subsequently, APV was washed out and synapses were mapped functionally. Very similar to TTX, APV abolished the clustering of functional synaptic inputs (Figure 6B), indicating that sorting functional inputs along developing dendrites is mediated by network firing activity and NMDA mediated synaptic plasticity.

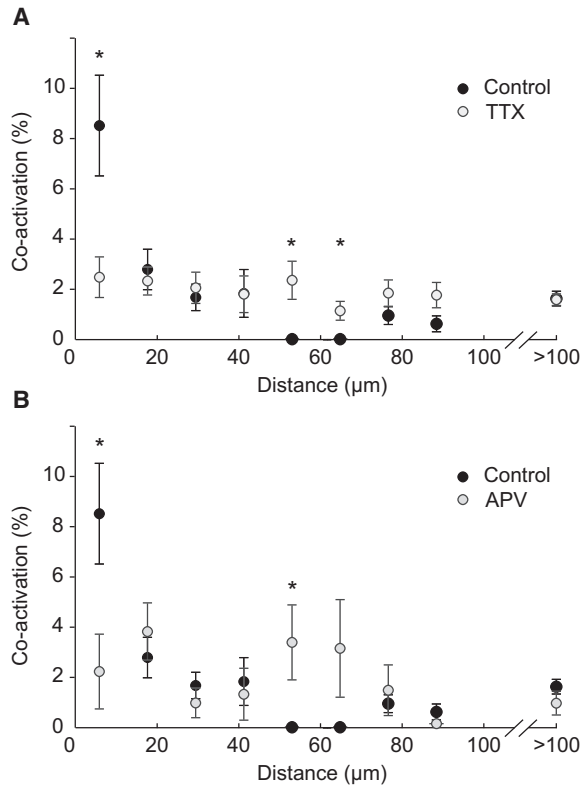

Figure 6. Synaptic Clustering Requires Neuronal Activity

(A) In control cells, synapses that were located close to each other showed high rates of coactivation and synapses with intermediate intersynaptic distances exhibited particularly low levels of coactivation. In cells that were incubated with TTX, the relationship between distance and coactivation was entirely absent. Asterisks indicate significant differences between coactivation values of control and TTX treated cells for given intersynapse distances.

(B) Like TTX, the treatment with the NMDA receptor antagonist APV abolished synaptic clustering. Control values are taken from (A). All error bars represent SEM.

DISCUSSION

The patterns of synaptic activation received by a developing neuron are crucial for the fine-tuning of its synapses. Here, we mapped the spatiotemporal activity patterns of large populations of synaptic inputs onto hippocampal pyramidal cells using calcium imaging combined with patch-clamp recordings. Our analysis gave several new insights into the fine-scale synaptic organization during development. First, we found that different sets of synapses are activated during successive bursts of synaptic inputs. Second, even though activation patterns vary from burst to burst, they are not completely random: synapses that are located close to each other are much more likely to be coactive than more distant ones. Third, the emergence of this fine-scale input organization requires spiking activity and NMDA receptor activation. Finally, probing the "functional synaptome" of individual cells, as a complementary approach to the structural synaptome (DeFelipe, 2010), may become an important tool for determining normal network development and its aberrations in transgenic animals or models of neurodevelopmental diseases.

Calcium imaging has been used widely to measure activity at individual synapses, mostly in spines (Chen et al., 2011; Denk et al., 1996; Murphy et al., 1994; Zito et al., 2009), but also in spineless dendrites (Goldberg et al., 2003; Katona et al., 2011; Murphy et al., 1995; Murthy et al., 2000). We found that synaptic calcium transients can be identified and separated reliably from nonsynaptic calcium transients across the entire dendritic arborization by simultaneous patch-clamp recordings in voltage-clamp mode. We also showed that our approach reveals a purely glutamatergic population of synapses, which allowed mapping excitatory synapses without pharmacological identification, making imaging the synaptome fast and—in fact—possible. We had also considered mapping the inhibitory synaptome by increasing the chloride reversal potential, such that GABAergic transmission would mediate inward currents, trigger local depolarization, and open voltage gated calcium channels. However, for a number of reasons, an important one being the need to separate GABAergic and glutamatergic transmission with time consuming pharmacological means making large volume maps unfeasible, we decided to restricted our analysis here to the excitatory synaptome, i.e., glutamatergic synapses.

Besides being instrumental for identifying specific spatiotemporal input patterns impinging onto the dendrites of developing

neurons, we expect that our approach will also be useful for comparing synaptic function between neurons during different developmental states and of different subclasses, genetic backgrounds, or from models of neurological disorders. While the structure of individual neurons has been routinely quantified for such purposes, the "synaptic state" of neurons has not been mapped with the spatiotemporal resolution described here. For example, we see great potential in deciphering the role of specific proteins in synaptic development and developmental plasticity. Furthermore, in neurodevelopmental diseases some connections are functionally aberrant whereas others are normal (Gibson et al., 2008). To identify the specific functional aberrations imaging the synaptome may become highly beneficial.

The most striking observation from our analysis of the developing "synaptome" is the strong relationship between the function of individual synapses and their location. Specifically, synapses that are located within a distance of 16 μm from each other are much more likely to be coactive than synapses that are further apart. We considered possible causes underlying coactivation of neighboring synapses. First, we tested whether individual axons might form multiple synapses at nearby positions along the dendrite. Our analysis of fluorescently labeled axons and dendrites shows, however, that each axon makes maximally one synapse on a given dendritic stretch of hippocampal neurons at this age. Furthermore, data from previous studies indicate that even in mature animals, where synapse densities are much higher than in our neonatal preparation, hippocampal axons form only one to five synapses with any postsynaptic pyramidal cell and only very rarely more than one functional bouton with a single dendrite (Pavlidis and Madison, 1999; Sorra and Harris, 1993). We show, in addition, that minimal stimulation of presynaptic axons never activates two neighboring synapses, confirming that clustering is not due to multiple synapses from the same axon. Moreover, this experiment demonstrates that spill-over of glutamate or diffusion of other signaling factors from one activated synapse to its neighboring sites is not a common phenomenon in the developing hippocampus and is therefore unlikely to contribute to the coactivation of neighboring synapses. Finally, we find that neither structural synapses—as labeled with an anti-synapsin antibody—nor functionally mapped synapses are clustered along dendrites, ruling out that a heterogeneous distribution of synapses may underlie local coactivation. Therefore, we conclude that functionally related axons frequently form neighboring synapses along developing dendrites.

To our knowledge, this is the first experimental demonstration of a subcellular connectivity precision with single synapse resolution. Interestingly, exactly this pattern of connectivity had been predicted on theoretical grounds previously (Poirazi and Mel, 2001). The prediction was related to the idea that neurons can compute information in independent subunits, such as individual dendritic stretches. This idea has received both theoretical as well as experimental support. For example, computer models predict that neurons, which can use dendrites as independent information processing units, would provide dramatically increased information processing and storage capacities (Govindarajan et al., 2006; Mel and Schiller, 2004). Furthermore, experiments in cortical pyramidal neurons demonstrated that their dendrites integrate synaptic depolarizations supralinearly, if they occur at neighboring sites (Losonczy and Magee, 2006; Nevian et al., 2007; Polsky et al., 2004), a prerequisite for local dendritic computations. Finally, learning processes can lead to the structural clustering of synapses on dendrites, e.g., in the owl auditory system (McBride et al., 2008). Together, this and other evidence make a convincing case that certain types of neurons boost their information processing capacity by taking advantage of independent dendritic computational units. However, as an additional requirement, the development of synaptic connections must be more specific than just connecting the right axon with the right neuron: each axon has to be connected to an appropriate dendritic branch or segment. The prediction was that this is achieved by connecting preferentially those axons to a common dendritic segment whose activity is temporally correlated (Govindarajan et al., 2006; Mehta, 2004; Poirazi and Mel, 2001). Our findings as described above now support this prediction: synaptic inputs that are correlated are located nearby on dendritic branches.

Beyond the theoretically expected clustering of functional inputs on developing hippocampal dendrites, mapping the developing synaptome revealed that synaptic pairs with intermediate intersynapse distances are even less correlated than those that are located on very distant branches. Future experiments will have to determine, whether this phenomenon reflects a depletion of correlated synapses at intermediate distances due to the clustering of correlated synapses at specific sites, or whether an active process is responsible for connecting inputs carrying diverse information to different locations of the same dendrite. Independently of the precise mechanism, the reduced correlation between synapses at intermediate distances helps sharpening the input-characteristics of developing hippocampal dendrites.

We furthermore show that the clustering of synaptic inputs requires action potential activity. Our experiments do not directly address the question, whether neuronal activity is required for the maintenance or the de novo formation of clustered inputs. Nevertheless, since only very few synapses are active at the age when we prepare the slices, most synapses emerge during the incubation and thus the de novo formation of clusters is probably prevented in the absence of spiking.

As a mechanism for the activity dependent clustering of synaptic inputs we propose a correlation based form of synaptic plasticity that incorporates spatial vicinity as one parameter. We find here that NMDA receptor signaling is required for setting up clustered connectivity. Furthermore, the extent of calcium diffusion from individual synaptic sites is similar to the distances between coactive synapses. Therefore, NMDA receptor mediated calcium influx, or NMDA triggered local activity of molecular factors, such as Ras (Harvey et al., 2008), may help stabilizing neighboring synapses that are coactive. In addition, inputs whose firing is uncorrelated with their neighbors' activity may get eliminated. Indeed, dendrites of hippocampal neurons exhibit such local plasticity mechanisms (Engert and Bonhoeffer, 1997; Govindarajan et al., 2011; Harvey and Svoboda, 2007; Sjöström and Häusser, 2006). Interestingly, the spatial range of a recently described local plasticity rule (10 μm intersynapse

distance; Harvey and Svoboda, 2007) is similar to the typical distances between coactive synapses in our study. Together our data show that spontaneous activity, which is present in essentially all developing neuronal networks, is an important component in the precise wiring of neural networks as it is capable of connecting neurons even with subcellular precision.

EXPERIMENTAL PROCEDURES

Cultures

All experimental procedures were carried out in compliance with the guidelines of the institutional animal care and use committee of the Royal Netherlands Academy of Arts and Sciences and the Max Planck Society. Organotypic slice cultures were prepared from newborn Wistar rats (P 0–2) according to the method of Stoppini et al. (1991). The animals were decapitated quickly and brains placed in ice-cold Gey's balanced salt solution (Life Technologies) under sterile conditions. Transversal slices (400 μm) were cut using a tissue chopper (McIlwain) and incubated with serum-containing medium on Millicell culture inserts (CM, Millipore). In these slice cultures the input connections of CA3 pyramidal cells from (1), granule cells of the dentate gyrus; (2), neighboring (but not contralateral, i.e., commissural) CA3 pyramidal cells; and (3), local interneurons are organotypically maintained, whereas the connections from outside the hippocampus, mainly those provided by the perforant path that originate in the entorhinal cortex and terminate on the distal apical dendrites of CA3 pyramidal cells within the *stratum lacunosum-moleculare* are absent.

Patch-Clamp Recordings

Experiments were performed after 2–4 days of incubation in visually identified CA3 pyramidal neurons using a MultiClamp 700B amplifier connected to a Digidata 1440A controlled by P-CLAMP 10 (Axon Instruments, Foster City, CA).

The recording chamber was temperature controlled at 35°C and perfused with Hank's balanced salt solution composed of: 3.26 mM $CaCl_2$, 0.493 mM $MgCl_2$, 0.406 mM $MgSO_4$, 5.33 mM KCl, 0.441 mM KH_2PO_4, 4.17 mM $NaHCO_3$, 138 mM NaCl, 0.336 mM Na_2HPO_4, and 5.56 mM D-glucose.

Synaptic currents were recorded in the whole-cell patch-clamp configuration using micropipettes (GB150TF-8P, Science Products, Hofheim, Germany) with a resistance of 3–5 MΩ filled with internal solution containing 12 mM KCl, 130 mM Kgluconat, 10 mM HEPES, 4 mM Mg-ATP, 8 mM NaCl, 33 μM Oregon Green BAPTA I; pH was adjusted to 7.2 with KOH and osmolarity to 290 mOsm. Cells were held at a potential of −55 mV. Recordings were discarded when the series resistance increased above 25 MΩ. To stimulate presynaptic axons, patch glass pipettes filled with external solution were placed in stratum radiatum and stimulation pulses (square, 0.5 ms) were adjusted (3–6 μA) to evoke synaptic currents.

Imaging

Images were acquired using a CCD camera (Andor iXon+ controlled by Andor Solis 4.4 software, Andor Technology, Belfast, Northern Ireland) mounted on a BX51WI microscope with a 40×/0.8 cone dipping water immersion objective (Olympus, Tokyo, Japan). The covered area was 208 × 208 μm. For low noise imaging at a rate of 30 Hz the camera was cooled to −70°C.

To acquire consecutive frames at different z planes we mounted a piezo-stepper (P-721.LLQ, Physik Instrumente, Karlsruhe, Germany) between microscope and objective. A trigger signal of the camera given at the beginning of each frame was used to move the piezo stepper controlled by an LVPZT controller (E-625.LR, Physik Instrumente) to the next z position. We recorded from three different z planes separated by 10 μm, thus resulting in a temporal resolution of 10 Hz.

To precisely register the electrophysiological with the optical recordings in time we recorded the trigger signal given by the camera at the beginning of every frame as a separate trace in the electrophysiological recording. Automated counting of trigger signals allowed then to determine exactly the beginning of every single frame of the calcium imaging in the electrophysiological trace.

Analysis

Image analysis was carried out automatically by custom made MATLAB software. As a first step in the analysis process, each set of three images from different z positions was collapsed into one maximum projection image. All maximum projection images from one recording were collected in one stack. Next, an F_0 image was generated in which each pixel represented the median of all pixel values at this position throughout the stack. The F_0 image was top-hat filtered using a disk-shaped structure (radius, three pixels) to correct for uneven background brightness. All areas brighter than two times the SD of the F_0 pixel values and larger than 200 pixels were detected as dendrites. The F_0 image was also used to generate a $\Delta F/F_0$ stack by subtracting it from each frame of the stack and dividing the result by F_0. Next, we calculated the derivative in time of the $\Delta F/F_0$ stack using a 3D convolution filter. The derivative was eroded with a disk-shaped structure (radius, two pixels) and subsequently binarized using a threshold of 15% $\Delta F/F_0\ s^{-1}$. A calcium transient was defined as a minimum of ten connected pixels in the binarized stack.

The spatial center of individual calcium transients was defined as the pixel coordinates where the largest increase in fluorescence occurred within each signal. Where necessary, these positions were shift corrected across recordings. Next, calcium transients were assigned to specific dendritic sites whose locations along the dendrite were determined in an iterative process: in the first step the center of the first calcium transient in a given recording was estimated as described above. Subsequently, all transients that occurred within 4 μm distally or proximally from the center of the first transient along the dendrite were considered to be transients from the same site. The center coordinates of all these transients were averaged and this value was used as a refined locus for this site of activity for the second iteration. During the iterations, some transients were newly included or excluded from the population assigned to this particular site and its center location adapted slightly. The process was stopped after 20 iterations, when in fact no more changes occurred. Then the first transient in time that was not yet assigned to any site was used as a starting point for determining the next site of activity. Only sites where at least two transients occurred were considered for further analysis. On average 7.6 ± 5.4 signals were detected per site (mean ± SD).

After defining the sites of calcium activity across all imaged dendrites and for all recordings, these sites were identified as putative synapses or as nonsynaptic sites. The distinction was based on the percentage of calcium transients that occurred simultaneously with synaptic currents at each site. This percentage was compared to the probability of synchronous occurrence by chance, which was calculated by dividing the number of frames during which at least one synaptic current event was detected by the total number of frames. Sites were defined as synaptic, if the rate of coincidence between calcium transients and synaptic currents exceeded the chance level 1.5 times.

To measure the extension and duration of individual signals, the maximum brightness of each signal in the $\Delta F/F_0$ representation was determined and all connected pixels brighter than two-thirds of this maximum were considered to be part of the signal.

The distances between synapses were determined along dendrites in maximum projections of the dendritic arborization. From these maximum projections skeleton models of the dendrites were generated where knots were defined as branching points, end points, and synapses. Subsequently, a matrix representing the shortest distances between all pairs of knots was generated using the Floyd-Warshall algorithm. From this matrix the minimal distances between two given synapses were derived. To estimate the maximal error due to analyzing distances in 2D as compared to 3D representations we determined the mean angle in which the trajectory of individual dendrites deviated from the focal plane. We found this angle to be 8.5° ± 2.9°. Measuring in 2D thus results in an underestimation of distances of less than two percent.

For detection of spontaneous electrophysiological events a similar procedure as described above was used. The onsets of signals were detected in a convoluted trace (derivative) of the average filtered current trace. The threshold for signal detection was set at 3.5 times the noise level.

The occurrence of synaptic bursts caused by network-driven GDPs was detected using an adaptation of the Rank Surprise (RS) method (Gourévitch

and Eggermont, 2007). This method analyzes the observed interevent interval (IEI) between detected synaptic currents. Even though activity bursts lack a clear definition they can be described as a train of synaptic activity with a low IEI. The RS method therefore considers the rank sum of associated IEI values and compares it to the sum of the distribution of discrete, uniformly randomized IEI values. Thus, RS statistics are calculated that reflect the degree to which an IEI value differs from what is expected from an independent and uniformly distributed sequence. The first synaptic current in a series to have an RS value above 2 was considered as potential starting point of a synaptic burst. The end of a synaptic burst was then defined as the time point where the electrophysiological signal returned to baseline. This baseline value was determined by averaging the current level over a 500 ms period before the onset of a burst. Putative bursts were included for further analysis, if they carried a total electric charge of at least 1 SD above the mean electric charge of unitary synaptic currents.

Immunohistochemistry

Neurons that were used for post-hoc immunohistochemistry were loaded with the red fluorescent dye Alexa-594 hydrazide (300 μM, Invitrogen) in addition to the calcium indicator. After recording synaptic calcium transients, slices were immediately fixed in paraformaldehyde (4% in 0.1 M sodium phosphate buffer [PB]) and left overnight at 4°C. Next, the slices were rinsed for 3 hr with PB and then preincubated in a blocker solution (0.4% Triton X-100, 1.5% horse serum, 0.1% bovine serum albumin in phosphate buffer, 4°C overnight). To detect the location of synaptic sites the slices were then incubated with a primary antibody raised against synapsin-1 (rabbit anti-synapsin-I, Chemicon, dilution 1:500 in 0.4% Triton X-100, 1.5% horse serum and 0.1 M PB) and—for the double-labeling experiments—an antibody against GAD65 (mouse anti-GAD65, Chemicon, dilution 1:1,000) for 7–10 days at 4°C. After rinsing the slices were incubated with the secondary antibody (anti-rabbit-CY3 or anti-rabbit-CY5 and anti-mouse-Alexa 488, each 1:50 in 0.1PB at 4°C) for 2–3 days. Slices were imbedded with Mowiol and imaged with a SP5 confocal microscope using a 63×/1.4 oil objective (Leica, Mannheim). Putative synapses were identified as sites of spectral overlap of the dendrite with anti-synapsin-labeled structures (yellow pixels) in all rotational views of 3D reconstructions. After identifying the positions of synaptic calcium transients along each dendrite, we aligned the images of the live and fixed dendrite and determined the distance between each transient site and its nearest putative synapse. The same was concurrently done for randomly chosen positions along the dendrite in a blind manner.

SUPPLEMENTAL INFORMATION

Supplemental Information includes three figures and can be found with this article online at doi:10.1016/j.neuron.2011.10.015.

ACKNOWLEDGMENTS

We thank Nicole Stöhr for preparing and maintaining hippocampal slice cultures, Friedrich Förstner for help setting up a program for automated distance calculations, as well as Axel Borst, Tom Mrsic-Flogel, Christiaan Levelt, and Valentin Stein for valuable comments on the manuscript. This work received additional support from the Netherlands Organization for Scientific Research (C.L.).

Accepted: October 10, 2011
Published: December 21, 2011

REFERENCES

Ben-Ari, Y., Cherubini, E., Corradetti, R., and Gaiarsa, J.L. (1989). Giant synaptic potentials in immature rat CA3 hippocampal neurones. J. Physiol. *416*, 303–325.

Benson, D.L., Watkins, F.H., Steward, O., and Banker, G. (1994). Characterization of GABAergic neurons in hippocampal cell cultures. J. Neurocytol. *23*, 279–295.

Bollmann, J.H., and Engert, F. (2009). Subcellular topography of visually driven dendritic activity in the vertebrate visual system. Neuron *61*, 895–905.

Bonifazi, P., Goldin, M., Picardo, M.A., Jorquera, I., Cattani, A., Bianconi, G., Represa, A., Ben-Ari, Y., and Cossart, R. (2009). GABAergic hub neurons orchestrate synchrony in developing hippocampal networks. Science *326*, 1419–1424.

Branco, T., and Häusser, M. (2010). The single dendritic branch as a fundamental functional unit in the nervous system. Curr. Opin. Neurobiol. *20*, 494–502.

Chen, X., Leischner, U., Rochefort, N.L., Nelken, I., and Konnerth, A. (2011). Functional mapping of single spines in cortical neurons in vivo. Nature *475*, 501–505.

Cline, H. (2003). Sperry and Hebb: oil and vinegar? Trends Neurosci. *26*, 655–661.

DeFelipe, J. (2010). From the connectome to the synaptome: an epic love story. Science *330*, 1198–1201.

Denk, W., Yuste, R., Svoboda, K., and Tank, D.W. (1996). Imaging calcium dynamics in dendritic spines. Curr. Opin. Neurobiol. *6*, 372–378.

Engert, F., and Bonhoeffer, T. (1997). Synapse specificity of long-term potentiation breaks down at short distances. Nature *388*, 279–284.

Frotscher, M., Heimrich, B., and Schwegler, H. (1990). Plasticity of identified neurons in slice cultures of hippocampus: a combined Golgi/electron microscopic and immunocytochemical study. Prog. Brain Res. *83*, 323–339.

Galli, L., and Maffei, L. (1988). Spontaneous impulse activity of rat retinal ganglion cells in prenatal life. Science *242*, 90–91.

Garaschuk, O., Hanse, E., and Konnerth, A. (1998). Developmental profile and synaptic origin of early network oscillations in the CA1 region of rat neonatal hippocampus. J. Physiol. *507*, 219–236.

Gibson, J.R., Bartley, A.F., Hays, S.A., and Huber, K.M. (2008). Imbalance of neocortical excitation and inhibition and altered UP states reflect network hyperexcitability in the mouse model of fragile X syndrome. J. Neurophysiol. *100*, 2615–2626.

Goldberg, J.H., Tamas, G., Aronov, D., and Yuste, R. (2003). Calcium microdomains in aspiny dendrites. Neuron *40*, 807–821.

Goodman, C.S., and Shatz, C.J. (1993). Developmental mechanisms that generate precise patterns of neuronal connectivity. Cell Suppl. *72*, 77–98.

Gourévitch, B., and Eggermont, J.J. (2007). A nonparametric approach for detection of bursts in spike trains. J. Neurosci. Methods *160*, 349–358.

Govindarajan, A., Kelleher, R.J., and Tonegawa, S. (2006). A clustered plasticity model of long-term memory engrams. Nat. Rev. Neurosci. *7*, 575–583.

Govindarajan, A., Israely, I., Huang, S.Y., and Tonegawa, S. (2011). The dendritic branch is the preferred integrative unit for protein synthesis-dependent LTP. Neuron *69*, 132–146.

Harvey, C.D., and Svoboda, K. (2007). Locally dynamic synaptic learning rules in pyramidal neuron dendrites. Nature *450*, 1195–1200.

Harvey, C.D., Yasuda, R., Zhong, H., and Svoboda, K. (2008). The spread of Ras activity triggered by activation of a single dendritic spine. Science *321*, 136–140.

Häusser, M., and Mel, B. (2003). Dendrites: bug or feature? Curr. Opin. Neurobiol. *13*, 372–383.

Hsia, A.Y., Malenka, R.C., and Nicoll, R.A. (1998). Development of excitatory circuitry in the hippocampus. J. Neurophysiol. *79*, 2013–2024.

Hua, J.Y., and Smith, S.J. (2004). Neural activity and the dynamics of central nervous system development. Nat. Neurosci. *7*, 327–332.

Huberman, A.D., Feller, M.B., and Chapman, B. (2008). Mechanisms underlying development of visual maps and receptive fields. Annu. Rev. Neurosci. *31*, 479–509.

Jia, H., Rochefort, N.L., Chen, X., and Konnerth, A. (2010). Dendritic organization of sensory input to cortical neurons in vivo. Nature *464*, 1307–1312.

Katona, G., Kaszas, A., Turi, G.F., Hajos, N., Tamas, G., Vizi, E.S., and Rozsa, B. (2011). Roller coaster scanning reveals spontaneous triggering of dendritic spikes in CA1 interneurons. Proc. Natl. Acad. Sci. USA *108*, 2148–2153.

Katz, L.C., and Shatz, C.J. (1996). Synaptic activity and the construction of cortical circuits. Science *274*, 1133–1138.

Khalilov, I., Dzhala, V., Ben-Ari, Y., and Khazipov, R. (1999). Dual role of GABA in the neonatal rat hippocampus. Dev. Neurosci. *21*, 310–319.

Lang, S.B., Stein, V., Bonhoeffer, T., and Lohmann, C. (2007). Endogenous brain-derived neurotrophic factor triggers fast calcium transients at synapses in developing dendrites. J. Neurosci. *27*, 1097–1105.

Larkum, M.E., and Nevian, T. (2008). Synaptic clustering by dendritic signalling mechanisms. Curr. Opin. Neurobiol. *18*, 321–331.

Leinekugel, X., Khazipov, R., Cannon, R., Hirase, H., Ben-Ari, Y., and Buzsáki, G. (2002). Correlated bursts of activity in the neonatal hippocampus in vivo. Science *296*, 2049–2052.

Lohmann, C., and Bonhoeffer, T. (2008). A role for local calcium signaling in rapid synaptic partner selection by dendritic filopodia. Neuron *59*, 253–260.

Losonczy, A., and Magee, J.C. (2006). Integrative properties of radial oblique dendrites in hippocampal CA1 pyramidal neurons. Neuron *50*, 291–307.

McBride, T.J., Rodriguez-Contreras, A., Trinh, A., Bailey, R., and DeBello, W.M. (2008). Learning drives differential clustering of axodendritic contacts in the barn owl auditory system. J. Neurosci. *28*, 6960–6973.

Mehta, M.R. (2004). Cooperative LTP can map memory sequences on dendritic branches. Trends Neurosci. *27*, 69–72.

Mel, B.W., and Schiller, J. (2004). On the fight between excitation and inhibition: location is everything. Sci. STKE *2004*, PE44.

Murphy, T.H., Baraban, J.M., Wier, W.G., and Blatter, L.A. (1994). Visualization of quantal synaptic transmission by dendritic calcium imaging. Science *263*, 529–532.

Murphy, T.H., Baraban, J.M., and Wier, W.G. (1995). Mapping miniature synaptic currents to single synapses using calcium imaging reveals heterogeneity in postsynaptic output. Neuron *15*, 159–168.

Murthy, V.N., Sejnowski, T.J., and Stevens, C.F. (2000). Dynamics of dendritic calcium transients evoked by quantal release at excitatory hippocampal synapses. Proc. Natl. Acad. Sci. USA *97*, 901–906.

Nevian, T., Larkum, M.E., Polsky, A., and Schiller, J. (2007). Properties of basal dendrites of layer 5 pyramidal neurons: a direct patch-clamp recording study. Nat. Neurosci. *10*, 206–214.

O'Donovan, M., Ho, S., and Yee, W. (1994). Calcium imaging of rhythmic network activity in the developing spinal cord of the chick embryo. J. Neurosci. *14*, 6354–6369.

Pavlidis, P., and Madison, D.V. (1999). Synaptic transmission in pair recordings from CA3 pyramidal cells in organotypic culture. J. Neurophysiol. *81*, 2787–2797.

Poirazi, P., and Mel, B.W. (2001). Impact of active dendrites and structural plasticity on the memory capacity of neural tissue. Neuron *29*, 779–796.

Polsky, A., Mel, B.W., and Schiller, J. (2004). Computational subunits in thin dendrites of pyramidal cells. Nat. Neurosci. *7*, 621–627.

Safiulina, V.F., Fattorini, G., Conti, F., and Cherubini, E. (2006). GABAergic signaling at mossy fiber synapses in neonatal rat hippocampus. J. Neurosci. *26*, 597–608.

Sanes, J.R., and Yamagata, M. (2009). Many paths to synaptic specificity. Annu. Rev. Cell Dev. Biol. *25*, 161–195.

Sholl, D.A. (1953). Dendritic organization in the neurons of the visual and motor cortices of the cat. J. Anat. *87*, 387–406.

Sipilä, S.T., Huttu, K., Voipio, J., and Kaila, K. (2006). Intrinsic bursting of immature CA3 pyramidal neurons and consequent giant depolarizing potentials are driven by a persistent Na+ current and terminated by a slow Ca2+ -activated K+ current. Eur. J. Neurosci. *23*, 2330–2338.

Sjöström, P.J., and Häusser, M. (2006). A cooperative switch determines the sign of synaptic plasticity in distal dendrites of neocortical pyramidal neurons. Neuron *51*, 227–238.

Smith, M.A., Ellis-Davies, G.C., and Magee, J.C. (2003). Mechanism of the distance-dependent scaling of Schaffer collateral synapses in rat CA1 pyramidal neurons. J. Physiol. *548*, 245–258.

Sorra, K.E., and Harris, K.M. (1993). Occurrence and three-dimensional structure of multiple synapses between individual radiatum axons and their target pyramidal cells in hippocampal area CA1. J. Neurosci. *13*, 3736–3748.

Spruston, N. (2008). Pyramidal neurons: dendritic structure and synaptic integration. Nat. Rev. Neurosci. *9*, 206–221.

Stoppini, L., Buchs, P.-A., and Muller, D. (1991). A simple method for organotypic cultures of nervous tissue. J. Neurosci. Methods *37*, 173–182.

Triplett, J.W., Owens, M.T., Yamada, J., Lemke, G., Cang, J., Stryker, M.P., and Feldheim, D.A. (2009). Retinal input instructs alignment of visual topographic maps. Cell *139*, 175–185.

Wong, R.O.L., Chernjavsky, A., Smith, S.J., and Shatz, C.J. (1995). Early functional neural networks in the developing retina. Nature *374*, 716–718.

Yuste, R., Peinado, A., and Katz, L.C. (1992). Neuronal domains in developing neocortex. Science *257*, 665–669.

Zhao, X., Shoji, S., and Lau, P. (2005). Balanced GABAergic and glutamatergic synapse development in hippocampal neurons. Biochem. Biophys. Res. Commun. *330*, 1110–1115.

Zito, K., Scheuss, V., Knott, G., Hill, T., and Svoboda, K. (2009). Rapid functional maturation of nascent dendritic spines. Neuron *61*, 247–258.